

# QUANTIFYING MINORITY CARRIER LIFETIME AND COLLECTION EFFICIENCY OF SOLAR CELLS BY COMBINED OPTICAL AND ELECTRICAL CHARACTERISATION TECHNIQUES

Vincent Tsai\*, Christos Potamialis, Soňa Uličná, Martin Bliss, Thomas R. Betts, Ralph Gottschalg  
Centre for Renewable Energy Systems Technology (CREST), Wolfson School of Mechanical, Electrical and  
Manufacturing Engineering, Loughborough University, Loughborough, Leicestershire, LE11 3TU, UK

\*Tel.: +44 1509 635362, Email: [v.tsai@lboro.ac.uk](mailto:v.tsai@lboro.ac.uk)

**ABSTRACT:** This work presents the use of a combined measurement system for spectrally-resolved photoluminescence (PL), time-resolved photoluminescence (TRPL) and transient photocurrent decay (TPCD) to characterise the physical properties of solar cells and their materials. A physical model is proposed to quantify the localised carrier collection efficiency of solar cells from the measured localised minority carrier lifetime from TRPL measurements and the localised minority carrier diffusion time from TPCD measurements. A single excitation laser source is used to measure TRPL and TPCD at the same spot on the solar cell. Combined PL, TRPL and TPCD measurements are conducted on a CdS/CdTe and a CIGS sample. The resulting PL spectra for both samples show that the emission spectra can yield information on the material bandgap. TRPL and TPCD yield localised carrier lifetime and diffusion times of  $\tau_{TRPL}=3.91\text{ns}$  and  $\tau_{TPCD}=40.5\text{ns}$  respectively for the CdS/CdTe sample, and  $\tau_{TRPL}=2.45\text{ns}$  and  $\tau_{TPCD}=196.8\text{ns}$  respectively for the CIGS sample. The ratio between the  $\tau_{TRPL}$  and  $\tau_{TPCD}$  values is shown to be proportional to the localised carrier collection efficiency, yielding collection efficiencies of 21.97% and 7.93% for the CdS/CdTe and CIGS sample, respectively. The initial results show that the localised carrier collection efficiency may be affected by the sample's metal contact configuration. In short, this combined measurement approach can offer a novel and useful method of characterising the material quality of solar cells and the localised carrier collection efficiency of finished PV devices.

Keywords: carrier lifetime, diffusion, photoluminescence, CdTe, CIGS

## 1 INTRODUCTION

Characterisation of minority carrier lifetime in solar cells is important for the research and development of photovoltaic (PV) devices. Minority carrier lifetime usually indicates the quality of the semiconductor material in a solar cell and affects the overall efficiency of a PV device. However, there are other important factors which can limit the PV device efficiency such as carrier transport and collection at the contacts [1]. It is therefore important to experimentally characterise these parameters in order to gain a better understanding of the limiting factors.

Minority carrier lifetime can be directly measured by time-resolved photoluminescence (TRPL) through luminescence decay from radiative recombination [2]. Transient photocurrent decay (TPCD) measures the overall average effective carrier recombination, transport and collection processes [3][4]. Usually, different measurement systems are used for each individual characterisation technique with different excitation sources/methods. This can result in different areas of the sample being measured due to repositioning errors. Furthermore, different excitation source wavelengths can result in different layers of the sample being measured due to different penetration depths [5]. Therefore, it is difficult to directly compare and correlate the data from each measurement system to extract additional physical properties.

For example, the decay times measured from TRPL and TPCD using two separate measurement systems bear no direct correlation with each other if measured using different excitation sources or measurement spots. If TRPL and TPCD are measured at the same spot on the sample, a localised carrier collection efficiency can be extracted which yields additional information for the characterisation of solar cell performance.

As part of this work, a measurement system combining spectrally-resolved photoluminescence (PL), TRPL and TPCD has been developed [6]. Combined PL, TRPL and

TPCD measurements were conducted on CdS/CdTe and CIGS solar cells. A physical model is proposed to quantify the localised minority carrier lifetime and carrier collection efficiency of solar cells from the combined measurements. The proposed model extracts the localised minority carrier lifetime from TRPL measurements and the localised minority carrier diffusion time from TPCD measurements at the same spot on the solar cell. This is conducted using a single excitation laser source. In addition, spectrally-resolved PL is measured for both samples to characterise the material bandgap.

## 2 METHODOLOGY

### 2.1 The combined measurement system

This section briefly details the measurement system used, an extended description is published in [6]. Figure 1 shows the overall measurement system schematic. The excitation light source is a pulsed picosecond laser with a wavelength of 640nm. A 10× objective lens focusses the laser onto the sample. The resulting luminescence from the laser excitation of the sample is collected using the same objective lens. The 650nm dichroic mirror and a 650nm long pass filter is used to remove any remaining laser light going into the monochromator used for wavelength scanning or selection.

The system uses three photodetectors: An amplified InGaAs photodiode with an extended wavelength range (500nm-1700nm) and two photomultiplier tubes (PMT); one extended visible range (230-920nm) PMT and one NIR (950-1700nm) PMT.

In previously presented work, the NIR PMT was not yet operational [6]. The NIR PMT allows for TRPL measurements of samples such as CIGS and CZTS. The PMTs are connected to a time-correlated single photon counting (TCSPC) board to measure TRPL, while the photodiode is connected to a data acquisition card to measure spectrally-resolved PL.

For transient electrical measurements, the sample is connected to a digital sampling oscilloscope with a  $50\Omega$  input impedance via a matching SMA coaxial cable and probes.

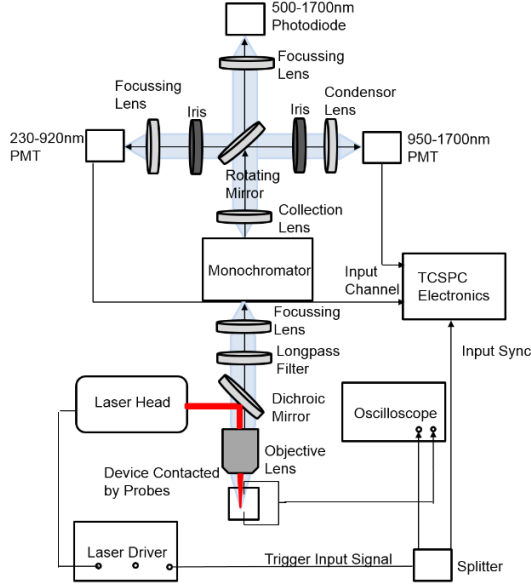


**Figure 1:** Overall measurement system schematic [6]

## 2.2 Sample fabrication

The test samples used during this work have been fabricated at CREST (see Figure 2). The CdS/CdTe sample is in the superstrate configuration. CdS was deposited on a  $50 \times 50$ mm substrate using a sono-chemical bath resulting in  $\sim 200$ nm thick films. CdTe was deposited by a close-space sublimation resulting in 4-6 $\mu$ m thick films. The CdS/CdTe devices were finished by depositing  $\sim 80$ nm of gold with an area of  $5 \times 5$ mm to act as the back contact. Further details on the CdS/CdTe device fabrication can be found in [7].

The solution-processed CIGS sample is in the substrate configuration using Mo/MoNx/Mo-coated soda lime glass as a back contact. The CIGS absorber layer thickness was  $\sim 3\mu$ m with a targeted composition of  $\text{Cu}_{0.9}\text{In}_{0.7}\text{Ga}_{0.3}\text{Se}_2$ . The CIGS device was completed by depositing CdS ( $\sim 80$  nm) using a chemical bath, followed by RF sputtering of intrinsic ZnO and Al doped ZnO (AZO) with a thickness of  $\sim 80$  and  $\sim 500$ nm, respectively. Finally, a top contact silver grid was evaporated and cells with an area of  $0.25\text{cm}^2$  were separated by mechanical scribing. Further details on the CIGS device fabrication can be found in [8]–[10].

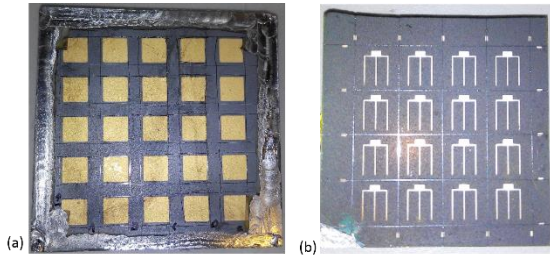


**Figure 2:** The (a) CdS/CdTe and (b) CIGS samples characterised in this work

## 3 THEORETICAL MODELS

### 3.1 Carrier recombination

Recombination of minority carriers in semiconductors is due to three main processes, Shockley-Read-Hall (SRH), radiative and Auger recombination [11]. This relation can be represented by rate equations and so the overall recombination rate is as follows:

$$\frac{dn}{dt} = \left(\frac{dn}{dt}\right)_{\text{SRH}} + \left(\frac{dn}{dt}\right)_{\text{rad}} + \left(\frac{dn}{dt}\right)_{\text{Auger}} \quad (1)$$

where  $n$  is the electron density and  $t$  is time. Eq.(1) can be calculated using the following equation [12][13]:

$$\begin{aligned} \frac{dn}{dt} = & -\frac{np - n_0p_0}{\frac{1}{A_n}(p + n_i) + \frac{1}{A_p}(n + n_i)} \\ & -B(np - n_0p_0) - C_n(np - n_0p_0)n \\ & -C_p(np - n_0p_0)p \end{aligned} \quad (2)$$

where  $n$  is the electron number density in the conduction band,  $p$  is the hole number density in the valence band,  $n_0$  and  $p_0$  are their values at equilibrium respectively,  $n_i$  is the intrinsic carrier density,  $A_n$  and  $A_p$  are the SRH recombination coefficients for electrons and holes respectively,  $B$  is the radiative recombination coefficient, and  $C_n$  and  $C_p$  are the Auger recombination coefficients for electrons and holes respectively. It is assumed in Eq.(2) that the energy level for the SRH recombination centre is located near the intrinsic Fermi level, which is usually located in the middle of the bandgap [14].

The p-type layer in the measured samples are thicker than the n-type layer by several orders of magnitude, as detailed in Section 2.2. Therefore, only the minority electrons in the p-type quasi-neutral region was considered in the physical model.

In the p-type layer, the majority carriers are holes which can be expressed as  $p \cong p_0 = N_A$  [1], where  $N_A$  is the doping concentration of the p-type acceptors and  $p_0$  is the hole number density at equilibrium. The hole number density  $p$  is greater than the electron number density  $n$ , (i.e.  $p \gg n$ ) which can be represented by  $n(t) = n_0 + \Delta n(t)$  [15] where  $n_0$  is the electron number density at equilibrium and  $\Delta n$  is the excess electron number density. It is assumed that the excess electron number density is greater than the electron number density at equilibrium (i.e.  $\Delta n(t) \gg n_0$ ). Therefore  $n_0$  can simply be neglected (i.e.  $n(t) \cong \Delta n(t)$ ) and Eq.(2) can then be simplified to [13]:

$$\frac{d\Delta n}{dt} = -(A_n + BN_A + C_pN_A^2 + C_nN_A\Delta n)\Delta n \quad (3)$$

Eq.(3) is a non-linear differential equation and can only be solved by numerical methods. Therefore, it is not suitable for fitting TRPL data because many physical parameters need to be known in advance. However, Eq.(3) can be simplified by assuming the low-injection condition, where the excess minority carrier concentration is less than the acceptor concentration (i.e.  $\Delta n \ll N_A$ ). The  $C_nN_A\Delta n$  term can be neglected and thus Eq.(3) can be simplified to:

$$\frac{d\Delta n(t)}{dt} = -\frac{\Delta n(t)}{\tau_n} \quad (4)$$

where  $\tau_n$  is the minority carrier lifetime represented as [2]:

$$\tau_n = \frac{1}{A_n + BN_A + C_p N_A^2} \quad (5)$$

The general solution of Eq.(4) is:

$$\Delta n(t) = \Delta n(0)e^{-t/\tau_n} \quad (6)$$

It should be noted that the  $C_n N_A \Delta n$  term cannot be neglected in the case of the high injection condition  $\Delta n \approx p_0 = N_A$  (i.e. at the initial stage of the carrier decay process). In this case, if  $C_n N_A \Delta n$  term is assumed to be a constant value, then Eq.(3) will become:

$$\frac{d\Delta n(t)}{dt} = -\frac{\Delta n(t)}{\tau_{\Delta n}} \quad (7)$$

where  $\tau_{\Delta n}$  is the minority carrier lifetime at high injection conditions and is represented by:

$$\tau_{\Delta n} = \frac{1}{A_n + BN_A + C_p N_A^2 + C_n N_A \Delta n} \quad (8)$$

The general solution of this equation is:

$$\Delta n(t) = \Delta n(0)e^{-t/\tau_{\Delta n}} \quad (9)$$

If Eqs.(5) and (8) are compared, it can be concluded that the value of  $\tau_{\Delta n}$  is less than  $\tau_n$ :

$$\tau_{\Delta n} < \tau_n \quad (10)$$

In short, Eq.(8) describes the decay regime of the initial high injection conditions in the carrier decay process, while Eq.(5) describes the decay regime approaching equilibrium of the low injection condition. As a result, the overall decay process is the sum of these two regimes which can be described as follows:

$$\Delta n(t) \approx \Delta n_1 e^{-t/\tau_{\Delta n}} + \Delta n_2 e^{-t/\tau_n} \quad (11)$$

where  $\Delta n_1$  and  $\Delta n_2$  are the excess carrier densities for the high and low injection regimes, respectively. In short, there are two carrier lifetime constants which can be obtained from the TRPL measurement:  $\tau_{\Delta n}$ , the carrier lifetime under the initial high injection conditions, and  $\tau_n$ , the carrier lifetime under low injection conditions. Since solar cells normally operate under low injection conditions,  $\tau_n$  was interpreted as the carrier lifetime. The minority carrier lifetime  $\tau_n$  is therefore represented as  $\tau_{TRPL}$ :

$$\tau_{TRPL} = \tau_n = \frac{1}{A_n + BN_A + C_p N_A^2} \quad (12)$$

### 3.2 Carrier lifetime from TRPL

TRPL directly detects the photon flux which is generated from radiative carrier recombination [15] and can be expressed by the following equation:

$$\varphi_{PL} \propto B(np - n_0 p_0) \quad (13)$$

where  $B$  is the radiative recombination coefficient.

Since the n-type layer is much thinner compared to the p-type layer of the samples in this work, it can be assumed that the output photon flux seen in the PL emission signal is from the p-type quasi-neutral region. As discussed in Section 3.1, in the p-type quasi-neutral region, the majority carriers  $p$  can be expressed as  $p \approx p_0 = N_A$ . The minority carriers  $n$  can be expressed as  $n = n_0 + \Delta n$ , where  $\Delta n$  is the excess electron number density [15]. These two expressions can then be substituted into Eq.(13):

$$\varphi_{PL} \propto BN_A \Delta n(t) \quad (14)$$

The detected PL signal  $\varphi_{PL}$  is therefore linearly proportional to the excess minority electron density  $\Delta n$ . The resulting TRPL data can be fitted by a double exponential decay function:

$$\varphi_{PL}(t) = a_1 e^{-t/\tau_1} + a_2 e^{-t/\tau_2} \quad (15)$$

where  $a_1$  and  $a_2$  are parameters for the amplitudes,  $t$  is time and  $\tau_1$  and  $\tau_2$  are parameters for the exponential time constants. Eq.(15) is identical to Eq.(11), where  $a_1 = \Delta n_1$ ,  $a_2 = \Delta n_2$ ,  $\tau_1 = \tau_{\Delta n}$  and  $\tau_2 = \tau_n$ , where  $\tau_1 < \tau_2$  according to Eq.(10).

In short, the longer decay time in the TRPL measurement  $\tau_2 = \tau_n$  describes the decay process approaching equilibrium under low injection conditions. This carrier lifetime is related purely to the material properties and is independent of the excess carrier density as indicated by Eq.(5). On the contrary, the shorter decay time in the TRPL measurement  $\tau_1 = \tau_{\Delta n}$  describes the initial decay process under high injection conditions. Its value is dependent on the excess carrier density as indicated by Eq.(8). Therefore,  $\tau_1 = \tau_{\Delta n}$  cannot represent the material properties and  $\tau_2 = \tau_n$  represents the localised carrier lifetime of the TRPL measurement.

### 3.3 Carrier diffusion time from TPCD

It was given that the measured TPCD signal comes from the p-type quasi-neutral region by assuming that the contributions from the space charge region and n-type quasi neutral region are negligible due to the very thin n-type CdS layer used in the samples. The minority electron number density  $n$  obeys the diffusion-recombination continuity equation as follows [14]:

$$\frac{\partial n}{\partial t} = D_n \frac{\partial^2 n}{\partial x^2} + g - r = 0 \quad (16)$$

where  $D_n$  is the electron diffusion coefficient,  $g$  and  $r$  are the generation and recombination rates. The spatially dependent partial differential equation can be transformed into a spatially independent rate equation in which all the physical quantities discussed below are presumed to be spatially averaged.

Minority carriers are generated from the absorption of the input photon flux. Therefore, the generation rate is as follows [16]:

$$g = \alpha \varphi = \left( \frac{dn}{dt} \right)_{gen} \quad (17)$$

where  $\alpha$  is the absorption coefficient and  $\varphi$  is the input photon flux. The recombination rate  $r$  is a combination of SRH, radiative and Auger recombination which can be described by a single value of the average minority carrier

lifetime  $\langle \tau_n \rangle$ , as follows:

$$-r = \left( \frac{dn}{dt} \right)_{rec} = -\frac{n - n_0}{\langle \tau_n \rangle} \quad (18)$$

where  $n_0$  is the minority carrier electron number density at equilibrium (i.e. no injection). It should be noted that  $\langle \tau_n \rangle$  is the average carrier recombination lifetime along the diffusion path, which is different from the localised carrier lifetime measured from the TRPL. The diffusion process in Eq.(16) can be represented by the minority carrier diffusion time  $\tau_{diff}$  as follows:

$$D_n \frac{\partial^2 n}{\partial x^2} \rightarrow \left( \frac{dn}{dt} \right)_{diff} = -\frac{n - n_0}{\tau_{diff}} \quad (19)$$

As a result, the partial differential equation of Eq.(16) can be represented by the following rate equations:

$$\frac{dn}{dt} = \left( \frac{dn}{dt} \right)_{gen} + \left( \frac{dn}{dt} \right)_{rec} + \left( \frac{dn}{dt} \right)_{diff} \quad (20)$$

It should be noted that in the actual TPCD measurement system, there are other factors which could possibly affect the measurement such as the PV device's junction capacitance and the measurement system capacitance in some cases. The advantage of using this rate equation approach is because it can be expanded further to accommodate other factors as follows:

$$\begin{aligned} \frac{dn}{dt} = & \left( \frac{dn}{dt} \right)_{gen} + \left( \frac{dn}{dt} \right)_{rec} + \left( \frac{dn}{dt} \right)_{diff} \\ & + \left( \frac{dn}{dt} \right)_{SCR} + \left( \frac{dn}{dt} \right)_{RC} + \dots \end{aligned} \quad (21)$$

where 'SCR' represents the junction capacitance from the space charge region and 'RC' represents the measurement system capacitance which is the electronic response time of the measurement system. However, these two factors will be ignored in this work for simplicity. The 'diff', 'SCR' and 'RC' terms in Eq.(21) are carrier transport processes and can be summed to form an overall collection rate, which is different from the generation and recombination processes as follows:

$$\begin{aligned} \left( \frac{dn}{dt} \right)_{col} = & \left( \frac{dn}{dt} \right)_{diff} + \left( \frac{dn}{dt} \right)_{SCR} + \left( \frac{dn}{dt} \right)_{RC} \\ = & -\frac{n - n_0}{\tau_{col}} \end{aligned} \quad (22)$$

where the collection time  $\tau_{col}$  is introduced to account for the time for electrons travelling from the point of generation across the sample to the metal contacts and then the measurement system to become a detected current signal. Therefore, the detected current signal  $J_{TPCD}(t)$  is linearly proportional to the carrier collection rate in Eq.(22) as follows:

$$J_{TPCD}(t) = qL \frac{n(t) - n_0}{\tau_{col}} \quad (23)$$

where  $q$  is the electron charge and  $L$  is the distance of the carrier diffusion path from the excited area to the metal

contact.

The overall rate equation for the transient photocurrent decay is formed by combining Eqs. (17), (18) and (22):

$$\frac{dn(t)}{dt} = \alpha\varphi(t) - \frac{n(t) - n_0}{\langle \tau_n \rangle} - \frac{n(t) - n_0}{\tau_{col}} \quad (24)$$

Eq.(24) is the sum of the charge carrier generation, recombination, and collection processes. Since the excitation is a pulsed source, the photon flux  $\varphi(t) = 0$  is assumed for  $t \geq 0$ . The decay from TPCD is measured and fitted after the excitation pulse so there will be no contribution to the generation at  $t \geq 0$  in the decay process and the  $\alpha\varphi(t)$  term can be omitted from Eq.(24):

$$\begin{aligned} \frac{dn(t)}{dt} = & -\frac{n(t) - n_0}{\langle \tau_n \rangle} - \frac{n(t) - n_0}{\tau_{col}} \\ = & -\frac{n(t) - n_0}{\tau_{decay}}, \quad \text{for } t \geq 0 \end{aligned} \quad (25)$$

where the decay time  $\tau_{decay}$  is a combination of the carrier recombination and collection processes:

$$\frac{1}{\tau_{decay}} = \frac{1}{\langle \tau_n \rangle} + \frac{1}{\tau_{col}} \quad (26)$$

The solution of Eq.(25) is as follows:

$$n(t) = n(0)e^{-t/\tau_{decay}} + n_0 \quad (27)$$

where  $n(0)$  is the carrier number density at  $t = 0$  which depends on the injection level and  $\tau_{decay}$  is the decay time in the TPCD. Eq.(27) can be substituted into Eq.(23) and the detected TPCD signal will become:

$$\begin{aligned} J_{TPCD}(t) = & \frac{qLn(0)}{\tau_{col}} \exp\left(-\frac{t}{\tau_{decay}}\right) \\ = & J_{TPCD}(0) \exp\left(-\frac{t}{\tau_{decay}}\right) \end{aligned} \quad (28)$$

where  $L$  is distance of the carrier diffusion path from the excited area to the metal contact as shown by the diagram in Figure 3.

#### 3.4 Localised collection efficiency

As indicated by Eq.(26) the decay time measured by TPCD  $\tau_{decay}$  is determined by two factors: the average carrier lifetime  $\langle \tau_n \rangle$  along the diffusion path is in the ns range so cannot currently be resolved from the TPCD measurement. The current TPCD measurement setup can only detect the slower process of carrier collection  $\tau_{col}$  (10s to 100s ns range). Therefore:

$$J_{TPCD}(t) \approx J_{TPCD}(0) \exp\left(-\frac{t}{\tau_{col}}\right) \quad (29)$$

If the minority carrier collection process is assumed to be dominated by the minority carrier diffusion process, the contribution of the 'SCR' and 'RC' terms in Eq.(21) can be ignored. Therefore the collection time  $\tau_{col}$  is almost equal to the carrier diffusion time  $\tau_{diff}$ :

$$\tau_{col} \approx \tau_{diff} \quad (30)$$

The measured decay time by TPCD  $\tau_{TPCD}$  can therefore be represented by the minority carrier diffusion time  $\tau_{diff}$ :

$$\tau_{TPCD} \approx \tau_{diff} \quad (31)$$

It can be shown that the minority carrier diffusion time is determined by the distance  $L$  of the carrier diffusion path from the excited area to the metal contact, and the minority carrier diffusion coefficient  $D_n$  as:

$$\tau_{TPCD} \approx \tau_{diff} = \frac{L^2}{2D_n} = \frac{L^2}{2L_n^2/\tau_n} = \frac{\tau_n}{2} \frac{1}{\eta_{col}^2} \quad (32)$$

It should be noted that the relation  $L_n = \sqrt{\tau_n D_n}$  [1] is used in Eq.(32) where  $L_n$  is the minority carrier diffusion length,  $D_n$  is the diffusion coefficient and  $\tau_n$  is the minority carrier lifetime. In Eq.(32), the localised collection efficiency  $\eta_{col}$  is defined as:

$$\eta_{col} \equiv \frac{L_n}{L} = \sqrt{\frac{\tau_{TRPL}}{2\tau_{TPCD}}} \quad (33)$$

In which  $\tau_n = \tau_{TRPL}$  as described above in Section 3.3. It should be noted that the TRPL and TPCD measurements represent the localised physical quantities, which are measured at the same spot on the sample. The localised collection efficiency  $\eta_{col}$  is defined as the ratio between the diffusion length  $L_n$  and the distance of the diffusion path  $L$ , which characterises the percentage of the photogenerated carriers in the sample that have been transported and collected as a detected TPCD signal before the carriers recombine.

The merit of this combined measurement approach is thus demonstrated by Eq.(33) where the localised carrier lifetime is directly measured by TRPL and the localised carrier diffusion time is measured by TPCD at the same spot. The ratio between these two values will yield the localised carrier collection efficiency which can provide additional useful information on the PV device's performance. This localised carrier collection efficiency cannot be measured by separate measurement systems based on the physical model described above.

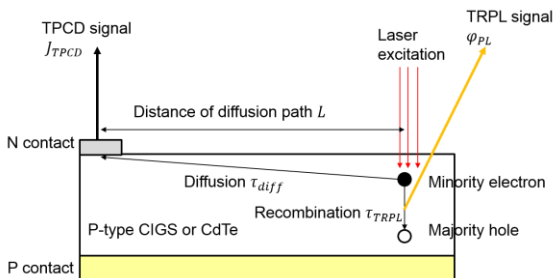


**Figure 3:** Illustration of the generation, recombination and collection processes of minority carriers in the measured samples.

#### 4 INITIAL RESULTS AND DISCUSSION

Combined measurements of PL, TRPL and TPCD were conducted on the two test samples described in

Section 2.2. The CIGS sample was measured to test the capability of the NIR PMT which was not previously operational. The CdS/CdTe sample has been measured in the previous work [6] and is used in this work to calculate the localised carrier collection efficiency.

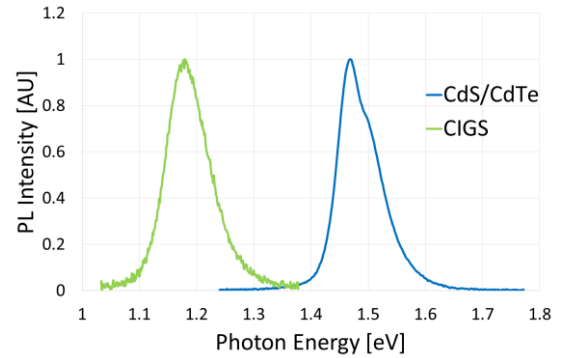
##### 4.1 Spectrally-resolved photoluminescence

Figure 4 shows the resulting PL spectra of the CdS/CdTe and CIGS sample. The laser excitation was pulsed at 2.5MHz for the CdS/CdTe sample and 40MHz for the CIGS sample to measure a detectable PL signal.

Qualitative analysis was conducted on the resulting PL spectra. The PL spectra have either one or two broad emission peaks which correspond to the material bandgaps, which are the main source of radiative band-to-band recombination.

The CdS/CdTe sample has two main emission peaks at  $\sim 1.47\text{eV}$  and  $\sim 1.50\text{eV}$ . The peak at  $1.50\text{eV}$  is attributed to the CdTe layer while the peak at  $1.47\text{eV}$  is attributed to the  $\text{CdS}_x\text{Te}_{1-x}$  layer. The formation of this  $\text{CdS}_x\text{Te}_{1-x}$  layer results from the diffusion of S into the CdTe layer, which is caused by the  $\text{CdCl}_2$  annealing treatment as detailed in [17][18].

The CIGS sample has one main broad emission peak at around  $\sim 1.18\text{eV}$  which is attributed to the luminescence from the p-type CIGS absorber layer, and is in the expected range of CIGS solar cells ( $1\text{-}1.7\text{eV}$ ) [19]. The CIGS p-type absorber layer has a tuneable bandgap by alloying  $\text{CuInSe}_2$  with either S or Ga [10] which changes the bandgap depending on the material composition ratio. When the  $\text{Ga}/(\text{Ga}+\text{In})$  ratio is between 25-30%, the bandgap is normally between  $1.1$  and  $1.2\text{eV}$  [20] as is observed in Figure 4.



**Figure 4:** Normalised PL spectra of a CdS/CdTe and CIGS sample

##### 4.2 Time-resolved photoluminescence

TRPL measurements were then conducted on the same spot as PL measurements without removing the samples. Figures 5 and 6 show the TRPL decay curves for the CdS/CdTe and CIGS sample respectively. The monochromator wavelength was set to the peak value of the PL emission spectrum: to  $846\text{nm}$  ( $1.47\text{eV}$ ) for the CdS/CdTe sample and to  $1055\text{nm}$  ( $1.18\text{eV}$ ) for the CIGS sample. The (230-920nm) PMT was used to measure the CdS/CdTe sample while the other (950nm-1700nm) PMT was used to measure the CIGS sample. The laser frequency was set at 2.5MHz for the CdS/CdTe sample and 20MHz for the CIGS sample.

A double exponential decay function was used to fit the two TRPL decay curves. The extracted values were ( $\tau_1 = 1.39\text{ns}$ ,  $\tau_2 = 3.91\text{ns}$ ) for the CdS/CdTe sample and ( $\tau_1 = 0.63\text{ns}$ ,  $\tau_2 = 2.45\text{ns}$ ) for the CIGS sample. As

discussed earlier in Section 3.4,  $\tau_1$  is the lifetime at the initial high injection condition and  $\tau_2$  is the lifetime at low injection condition. Therefore, the value  $\tau_2$  will be used as the  $\tau_{TRPL}$  value as it is the bulk recombination. It should also be noted that the TRPL decay curves did not have the instrument response function (IRF) deconvoluted which may result in slight overestimation of the measured carrier lifetime.

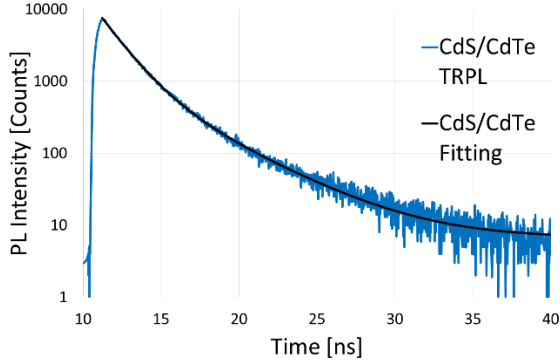


**Figure 5** Corresponding room temperature TRPL decay curves of the CdS/CdTe sample ( $\tau_1 = 1.39\text{ns}$ ,  $\tau_2 = 3.91\text{ns}$ ) measured at 846nm with 30s integration time

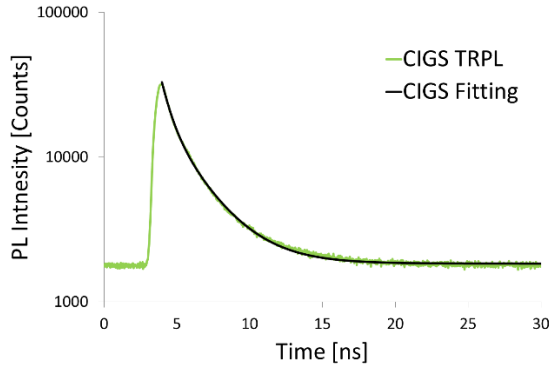


**Figure 6** Corresponding room temperature TRPL decay curves of the CIGS sample ( $\tau_1 = 0.63\text{ns}$ ,  $\tau_2 = 2.45\text{ns}$ ) measured at 1055nm with 30s integration time

#### 4.3 Transient photocurrent decay

TPCD measurements were conducted on the same area as the TRPL and PL on both samples (see Figures 7 and 8). During TPCD measurements, the PV device is contacted by probes which are connected to an oscilloscope. Each laser pulse creates excess carriers and thus generates a photovoltage. The subsequent decay is measured as a function of time and the minority carrier diffusion time  $\tau_{TPCD}$  can be extracted through fitting. A single exponential decay function (as described by Eq.(29)) was used to fit the two decay curves.  $\tau_{TPCD}$  values of 40.5ns and 196.8ns were extracted for the CdS/CdTe sample and the CIGS sample respectively.

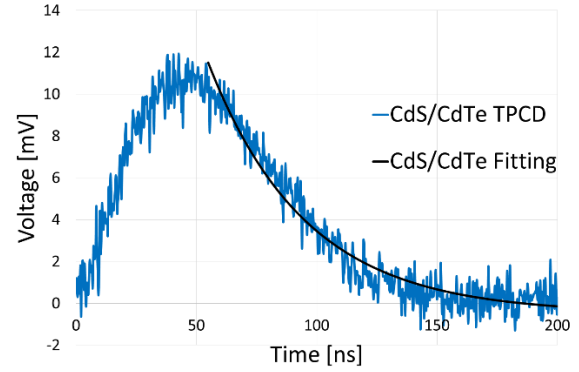


**Figure 7** Corresponding room temperature TPCD curves of the CdS/CdTe sample ( $\tau_{TPCD} = 40.5\text{ns}$ ) measured under 640nm wavelength and 2.5MHz frequency excitation without external biasing light

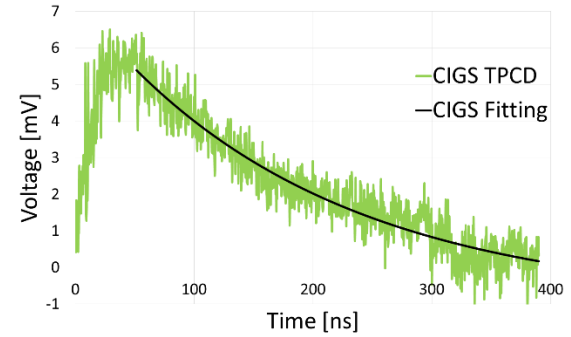


**Figure 8** Corresponding room temperature TPCD curves of the CIGS sample ( $\tau_{TPCD} = 196.8\text{ns}$ ) measured under 640nm wavelength and 2.5MHz frequency excitation without external biasing light

#### 4.4 The localised carrier collection efficiency

The localised carrier collection efficiency  $\eta_{col}$  was calculated for both samples using Eq.(33) and the fitted values  $\tau_{TRPL}$  and  $\tau_{TPCD}$  from TRPL and TPCD, respectively (see Table I).  $\eta_{col}$  is the percentage of generated carriers collected by the metal contacts which do not recombine during the transport process.

It should be noted that the measured power conversion efficiency (PCE)  $\eta$  of a device is better related to the 'global' carrier collection efficiency where the whole sample is illuminated by the incident light. On the contrary,  $\eta_{col}$  measured from the 'localised' carrier collection efficiency is directly linked to the small spot of the laser excitation. The measurement system is currently only a localised point-based measurement and not a spatially-resolved measurement. This means that the measured localised carrier collection efficiency is not exactly proportional to the power conversion efficiency and is possibly more sensitive to the sample's contact configuration as will be discussed below. Therefore, the localised collection efficiency can only be compared with the overall PCE if the samples have the same contact configuration and also measurement setup.

The localised carrier collection efficiency  $\eta_{col}$  calculated by Eq.(33) show that the CdS/CdTe's  $\eta_{col}$  is 21.97% and 7.89% for CIGS. The CdS/CdTe's localised collection efficiency is more than double than that of CIGS. It is initially speculated that one of the reasons is because the front and back contacts of the CdS/CdTe sample have a larger area and are also more densely

arranged than the CIGS sample. This means that there is a higher chance of the carriers being collected by the contact configuration of the CdS/CdTe sample measured here.

**Table I:** Fitted TRPL  $\tau_{TRPL}$  and TPCD  $\tau_{TPCD}$  values and calculated collection efficiencies  $\eta_{col}$

Sample	$\tau_{TRPL}$ (ns)	$\tau_{TPCD}$ (ns)	$\eta_{col}$ (%)
CdS/CdTe	3.91	40.5	21.97
CIGS	2.45	196.8	7.89

## 5 CONCLUSIONS AND FUTURE WORK

A combined measurement system of PL, TRPL and TPCD has been developed in this work. A physical model was proposed to quantify the localised carrier collection efficiency of solar cells from the measured localised minority carrier lifetime from TRPL measurements and the localised minority carrier diffusion time from TPCD measurements at the same spot on the solar cell. This is achieved by combined TRPL and TPCD measurements using a single excitation laser source. The localised collection efficiency is shown to be proportional to the ratio between the localised carrier lifetime and diffusion time.

Combined PL, TRPL and TPCD measurements were conducted on a CdS/CdTe and a CIGS sample. The initial results indicate that the localised carrier collection efficiency in this work is possibly affected by the sample's metal contact configurations and measurement setup. However, further investigation and measurements need to be conducted to verify this. This combined measurement approach can nevertheless offer a novel and useful method of characterising the material quality of solar cells and the localised carrier collection efficiency of the finished PV device.

The next steps in this work are to also examine the other factors which can affect the TPCD and TRPL measurements. For TPCD, external bias lighting will be applied to the sample during the TPCD measurement to observe the effect on the junction capacitance [21]. The signal-to-noise ratio and response time of the TPCD can also be improved. Furthermore, the IRF will be deconvoluted from the TRPL measurements to increase the accuracy of the extracted carrier lifetime values of TRPL.

Finally, the PL, TRPL and TPCD measurements are currently point-based measurements, an x-y scanning stage can be implemented for spatially-resolved measurements which in turn will provide further information on the point-by-point localised collection efficiency of the entire sample.

## 6 ACKNOWLEDGEMENTS

This work was supported by the UK Engineering and Research Council through the PVteam project EP/L017792/1: Photovoltaic Technology based on Earth Abundant Materials and by the EPSRC Centre for Doctoral Training in New and Sustainable Photovoltaics CDT-PV, EP/L01551X/1.

## 7 REFERENCES

- [1] J. Nelson, *The Physics Of Solar Cells*. London: Imperial College Press, 2003.
- [2] W. Metzger, R. Ahrenkiel, and P. Dippo, "Time-resolved photoluminescence and photovoltaics," in *Department of Energy Solar Energy Technologies Program Review Meeting*, 2004, vol. 1, no. January, pp. 1–2.
- [3] S. Wood, D. O. Connor, C. W. Jones, J. D. Claverley, J. C. Blakesley, C. Giusca, and F. A. Castro, "Transient photocurrent and photovoltage mapping for characterisation of defects in organic photovoltaics," *Sol. Energy Mater. Sol. Cells*, vol. 161, no. November 2016, pp. 89–95, 2017.
- [4] X. Wang, S. Karanjit, L. Zhang, H. Fong, Q. Qiao, and Z. Zhu, "Transient photocurrent and photovoltage studies on charge transport in dye sensitized solar cells made from the composites of TiO<sub>2</sub> nanofibers and nanoparticles," *Appl. Phys. Lett.*, vol. 98, no. 8, pp. 1–4, 2011.
- [5] D. Kuciauskas, J. N. Duenow, A. Kanevce, J. V. Li, M. R. Young, P. Dippo, and D. H. Levi, "Optical-Fiber-Based, Time-Resolved Photoluminescence Spectrometer for Thin-Film Absorber Characterization and Analysis of TRPL Data for CdS / CdTe Interface," in *Proceedings of the 38th IEEE Photovoltaic Specialist Conference*, 2011, pp. 1721–1726.
- [6] V. Tsai, F. Bittau, C. Potamialis, M. Bliss, T. R. Betts, and R. Gottschalg, "Combined Electrical and Optical Characterisation of Recombination Mechanisms and Minority Carrier Lifetime in Solar Cells," in *14th Photovoltaic Science, Applications and Technology Conference*, 2018, pp. 57–60.
- [7] C. Potamialis, F. Lisco, B. Maniscalco, M. Togay, J. W. Bowers, and J. M. Walls, "Process development of sublimated Cu-free CdTe solar cells," in *13th Photovoltaic Science, Application and Technology Conference*, 2017.
- [8] S. Uličná, P. Arnou, C. S. Cooper, V. Wright, Lewis D. Malkov, J. M. Walls, and J. W. Bowers, "A comparison of different selenisation approaches for Cu(In,Ga)(S,Se)<sub>2</sub> solar cells," in *13th Photovoltaic Science, Application and Technology Conference*, 2017.
- [9] S. Uličná, P. Arnou, A. Eeles, M. Togay, L. D. Wright, A. Abbas, V. Malkov, J. M. Walls, and J. W. Bowers, "Control of MoSe<sub>2</sub> formation in hydrazine-free solution-processed CIS / CIGS thin film solar cells," in *44th IEEE PVSC Conference*, 2017.
- [10] P. Arnou, C. S. Cooper, S. Uličná, A. Abbas, A. Eeles, L. D. Wright, A. V. Malkov, J. M. Walls, and J. W. Bowers, "Solution processing of CuIn(S,Se)<sub>2</sub> and Cu(In,Ga)(S,Se)<sub>2</sub> thin film solar cells using metal chalcogenide precursors," *Thin Solid Films*, vol. 633, no. October, pp. 76–80, 2017.
- [11] V. K. Khanna, "Physical understanding and technological control of carrier lifetimes in semiconductor materials and devices: A critique of conceptual development, state of the art and applications," *Prog. Quantum Electron.*, vol. 29, no. 2, pp. 59–163, 2005.
- [12] D. Alonso-Álvarez, T. Wilson, P. Pearce, M.

- Führer, D. Farrell, and N. Ekins-Daukes, "Solcore: a multi-scale, Python-based library for modelling solar cells and semiconductor materials," *J. Comput. Electron.*, vol. 17, no. 3, pp. 1–25, 2018.
- [13] D. Schroder, *Semiconductor Material and Device Characterization*, 3rd ed. New Jersey: John Wiley & Sons Ltd, 2006.
- [14] S. Sze and M.-K. Lee, *Semiconductor Devices: Physics and Technology*, 3rd ed. Wiley, 2013.
- [15] W. K. Metzger, D. Albin, D. Levi, P. Sheldon, X. Li, B. M. Keyes, and R. K. Ahrenkiel, "Time-resolved photoluminescence studies of CdTe solar cells," *J. Appl. Phys.*, vol. 94, no. 5, pp. 3549–3555, 2003.
- [16] W. K. Metzger, R. K. Ahrenkiel, J. Dashdorj, and D. J. Friedman, "Analysis of charge separation dynamics in a semiconductor junction," *Phys. Rev. B - Condens. Matter Mater. Phys.*, vol. 71, no. 3, pp. 1–9, 2005.
- [17] D. Kuciauskas, A. Kanevce, J. N. Duenow, P. Dippo, M. Young, J. V. Li, D. H. Levi, and T. a. Gessert, "Spectrally and time resolved photoluminescence analysis of the CdS/CdTe interface in thin-film photovoltaic solar cells," *Appl. Phys. Lett.*, vol. 102, no. 17, 2013.
- [18] A. Rohatgi, "A Study of Efficiency Limiting Defects in Polycrystalline CdTe/CdS Solar Cells," *Int. J. Sol. Energy*, vol. 12, no. 1–4, pp. 37–49, 1992.
- [19] V. Buschmann, H. Hempel, A. Knigge, C. Kraft, M. Roczen, M. Weyers, T. Siebert, and F. Koberling, "Characterization of semiconductor devices and wafer materials via sub-nanosecond time-correlated single-photon counting," *J. Appl. Spectrosc.*, vol. 80, no. 3, pp. 449–457, 2013.
- [20] M. Kemell, M. Ritala, and M. Leskelä, "Thin film deposition methods for CuInSe<sub>2</sub> solar cells," *Crit. Rev. Solid State Mater. Sci.*, vol. 30, no. 1, pp. 1–31, 2005.
- [21] H. Cui, J. Wang, C. Wang, C. Liu, K. Pi, X. Li, Y. Xu, and Z. Tang, "Experimental Determination of Effective Minority Carrier Lifetime in HgCdTe Photovoltaic Detectors Using Optical and Electrical Methods," *Adv. Condens. Matter Phys.*, vol. 2015, pp. 1–6, 2015.